Direct synthesis of dimethyl carbonate from methanol and carbon dioxide over nickel loaded ceria as improved catalysts

Mariyamuthu Mariyaselvakumar[1,2] · Tamilmani Selvaraj[3] ·
Viswanathan Balasubramanian[3] · Kannan Srinivasan[1,2]

Abstract

The direct synthesis of dimethyl carbonate (DMC) without a dehydrating agent is challenging but has a significant value. Here we demonstrate the catalytic activity of inexpensive nickel loaded ceria in both batch and continuous processes for this reaction. The prepared catalysts were characterized by various physicochemical characterization techniques. The nickel-loaded ceria catalysts exhibited good catalytic activity for the synthesis of DMC in good yield (4.6 mmol) and 100% selectivity. The yield obtained is nearly six times higher than pristine CeO_2, which clearly depicts the role of nickel. Reaction under high pressure continuous flow also provided a similar trend wherein a maximum yield of 15 mmol with 100% liquid phase selectivity of DMC was noted. Density functional theory calculations were carried out to investigate the adsorption energies of CO_2 and methanol on pristine ceria and Ni modified ceria. The high catalytic activity of Ni-modified catalyst was attributed to the presence of strong acidic and moderate basic sites as elucidated from temperature-programmed desorption and pyridine adsorption monitored via FT-IR studies. The experiment result revealed that the $Ce_xNi_{x-y}O_{2-\delta}$ could be a reusable and longer active catalyst for the direct synthesis of DMC.

✉ Kannan Srinivasan
skannan@csmcri.res.in; kanhem1@yahoo.com

1 Division of Inorganic Material and Catalysis, CSIR-Central Salt and Marine Chemicals Research Institute, Council of Scientific and Industrial Research (CSIR), GB Marg, Bhavnagar 364002, India

2 Department of Chemistry, Maharaja Krishnakumarsinhji Bhavnagar University, Bhavnagar 364001, India

3 National Centre for Catalysis Research, Indian Institute of Technology - Madras, Chennai 600036, India

🖄 Springer

Introduction

In the current environmental landscape, carbon dioxide (CO_2) emission has an indivisible relation with the global economy. Development of environmentally benign industrial processes utilizing the renewable C1 gaseous reagent (CO_2) for the production of value-added chemicals and fuels could act as an important balancing bridge between the economic and ecological policy [1]. Cleaner production projects deliver planned solutions for greener chemicals, sustainable materials, and safer products [2]. CO_2 being abundantly available and an inexpensive carbon source, its effective valorization has a great significance to alternate fossil-based resources [3, 4]. Great efforts have been made on both reductive and non-reductive transformations of CO_2 to methanol, formic acid, light alkanes, polyurethanes and inorganic/organic carbonates [5, 6]. Among them, organic carbonates have large industrial applications, thanks to high market potential, due to their application in pharmaceutical intermediates, agrochemicals, and engineered polymers. Dimethyl carbonate (DMC) has diverse industrial applications such as lubricants, electrolytes for lithium-ion batteries and in varnishes. Further, it is proposed as benign substitute for highly toxic phosgene or dimethyl sulfate in oxidative carbonylation and methylation reactions, respectively [7]. It is a promising octane booster [8], polar solvent, an intermediate in the synthesis of several organic compounds, and a potential oxygenate for transportation fuels [9, 10]. Conventionally, DMC was produced through a toxic phosgene route. However, recently phosgene-free technologies such as oxy-carbonylation of methanol, carbonylation of methyl nitrile and transesterification of ethylene carbonate have been industrially developed [11]. Direct synthesis of DMC from CO_2 and methanol is one of the attractive yet challenging ways to reduce greenhouse gases (GHG) emission besides CO_2 utilization [12]. The reaction was carried out initially using homogeneous catalysts like dibutyltindimethoxide and several organotin catalysts; however, the main disadvantage of these catalysts is decomposition, reusability and toxicity [7]. To overcome this problem, various metal oxides and mixed metal oxides based heterogeneous catalysts such as CeO_2, CeO_2–ZrO_2, $Ce_{0.6}$–$Zr_{0.4}O_2$, Mo–Cu–Fe/SiO_2, $Co_{1.5}PW_{12}O_{40}$, $Ce_{0.1}Ti_{0.9}O_2$, Cu–Ni/GNS, Mg–Al hydrotalcite/SiO_2, ZrO_2–MgO, graphene aerogel Cu–Ni, $Ce_{1-x}Mn_xO_2$ were reported for the synthesis of DMC [12–25]. Among them, CeO_2 and ceria-based oxides showed better catalytic activity due to their unique acid–base property and promoted in the selective formation of DMC from CO_2 [12, 26–28].

Furthermore, in contrast to the traditional batch system, very few were attempted to use a continuous system. The major concern in DMC synthesis is formation of water during the reaction which backslides the equilibrium. Thus, to overcome the equilibrium limitation and to improve the yield of DMC various dehydrating agents such as 2,2-dimethoxypropane, acetonitrile, 2-cyanopyridine, trimethyl orthoacetate have been reported [29]. In this work, we sought to enhance the activity of CeO_2 by introducing additional Lewis acid sites by loading the low cost and abundantly available Ni using a simple approach for

the direct synthesis of DMC without using any dehydrating agent. Subsequently, to investigate the catalytic activity of the developed catalyst for the production of DMC through batch and fixed bed continuous reactor systems. To the best of our literature knowledge (Supplementary Table S1), this is the first report on $Ce_xNi_{x-y}O_{2-\delta}$ catalyst, synthesized by the simple precipitation method at the ambient condition utilized upon DMC production from CO_2. Furthermore, computational methods were applied to calculate the adsorption binding energy of reactant on Ni modified ceria and bare Ce system.

Experimental procedure

Catalysts preparation

Ce–Ni mixed metal oxides with different Ni loadings were prepared by a co-precipitation method. A known amount of cerium precursor and different amounts of nickel precursor (0–80 mol%) were dissolved in deionised water to form a homogeneous solution. To this, the ammonia solution (1 M) was slowly added under continuous stirring till the pH reached 10, and it was then filtered and washed with deionized water. After drying the resulting product at 100 °C for 12 h, it was finally calcined at 600 °C for 4 h in air. The mixed metal oxide samples are named hereafter as $Ce_xNi_{x-y}O_{2-\delta}$, (or CN-X) and the amount of nickel loading was estimated by XPS analysis. For the sake of comparison ceria-based catalysts were also synthesized by conventional precipitation and impregnation methods the details of which are given in supporting information (SI).

Catalytic reaction procedure

Direct synthesis of DMC from methanol and carbon dioxide was conducted in a stainless steel (SS316) high pressure reactor having an internal volume of 100 mL (Autoclave Engineers, USA). In a typical experiment 20 g of methanol (625 mmol) and 0.5 g of catalyst were charged into the reactor, and was purged three times with UHP grade carbon dioxide. The reactor was then pressurized up to 40 bar using carbon dioxide and heated to the desired temperature. The contents in the reactor were stirred using an overhead mechanical four-blade turbine stirrer. After a stipulated time of reaction, the reactor was cooled to room temperature and depressurized. Biphenyl was added to the mixture in the reactor as an external standard. Reaction products were analyzed and quantified with a gas chromatography on a Varian 450 equipped with a HP-5 column and flame ionization detector (FID).

Catalyst characterization

Powder X-ray diffraction (PXRD) was carried out in a Rigaku—Miniflex II system using Cu K_α radiation ($\lambda = 1.5406$ Å). A step size of 0.04° with a step time of 2 s was used for data collection (scan speed, 1.2°/min). Fourier transform infrared (FT-IR)

absorption spectra of the samples were recorded in a Perkin-Elmer FT-IR spectrometer FT-1730. The powdered samples were ground with KBr in 1:20 weight ratio and pressed into pellets for recording the spectra. 25 spectra (recorded with a nominal resolution of 4 cm^{-1}) were accumulated and averaged to improve the signal to noise ratio. The basicity of the catalyst was measured using CO_2 temperature programmed desorption (TPD) on a Micrometrics Auto-Chem 2920 instrument. In a typical measurement, about 0.02 g of the powdered sample was placed in a quartz U-tube and degassed at 200 °C for 1 h in helium at a flow rate of 35 mL/min. After cooling to 80 °C, the gas was changed to CO_2 treated at the same temperature for 1 h. The gas was switched to helium at the same temperature and held at this temperature for 1 h, after this TPD was performed at 10 °C/min up to 800 °C. A thermal conductivity detector was used for the desorbed CO_2 quantification. Surface concentrations of acidic sites were determined by temperature-programmed desorption (TPD) technique using ammonia (NH_3) as a probe molecule on the same instrument. A similar procedure was adopted except for the gas being 5% NH_3 in helium. The Bronsted (B) and Lewis (L) acid sites of the catalysts are differentiated by pyridine adsorption using PerkinElmer GX spectrophotometer (DRIFT, Graseby Specac, P/N 19,900) and a temperature controller (Graseby Specac, P/N 20,130). X-ray photoelectron spectroscopy (XPS) studies were carried out using Thermo Scientific-NEXA high performance, automated X-ray photoelectron spectrometer. Delay line detector was used for all the studies using Al-Kα radiation (1486.6 eV) as the excitation source with the pass energy of 50 eV. The vacuum during measurements was better than 5×10^{-8} mbar and data reduction and processing were performed using AVANTAGE software. Raman spectra were recorded in the range 400–4000 cm^{-1} on a Nicolet NXR FT-Raman spectrometer system using He Ne laser (λ 532 nm) calibrated against the emission lines of Ne. Transmission electron microscope (TEM, - JEOL, JEM-2100 M) with an acceleration voltage of 200 keV using carbon-coated 200 mesh copper/gold grids.

Computational studies

DFT calculations were carried out in order to obtain information on the structures and adsorption energies of carbon dioxide and methanol on Ni loaded ceria. All the calculations have been performed at the B3LYP hybrid exchange–correlation functional level of theory [30–32]. For geometry optimization, we used SDD basis set that includes the Stuttgart-Dresden relativistic small core ECP basis set for metals and 6-31 g(d) basis set for the lighter atoms. The vibrational frequency analysis of the optimized geometry confirmed that the optimized geometry which corresponds to minima on the potential energy surface by exhibiting all real frequencies. All the calculations have been performed using the Gaussian 16 program package [33].
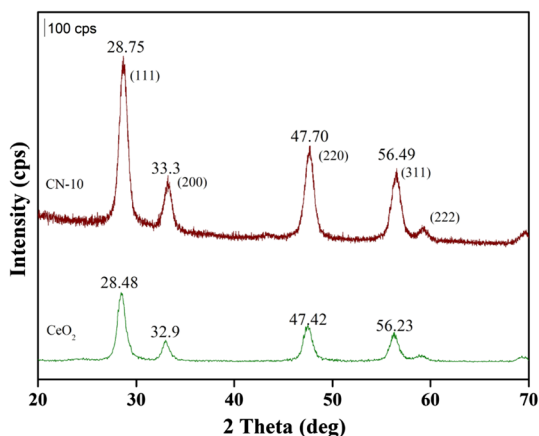
Result and discussion

All the PXRD patterns of the synthesized CeO_2 and $Ce_xNi_{x-y}O_{2-\delta}$ showed very similar well-resolved X-ray diffraction peaks that can be indexed to the face-centered cubic (FCC) fluorite structure of CeO_2 (JCPDS 34-0394). The powder X-ray diffraction patterns (PXRD) of the prepared catalysts are given in Fig. 1. The X-ray line broadening of the peaks at $2\theta = 28°$, 33°, 47° and 56° corresponding to (111), (200), (220), and (311) reflections indicate co-presence of Ce^{3+} and Ce^{4+} [34]. The PXRD of 10 mol% Ni loaded on ceria (calcined at 700 °C hereafter referred as CN-10) showed a pattern similar as that of CeO_2, and the 2θ value of 43.3° is corresponds to the NiO. However, with the corresponding 2θ values of Ceria is shifted slightly to higher values owing to nickel addition as indicated in Fig. 1 [35].

The prepared different Ni loaded ceria catalysts were characterized by FT-IR spectroscopy and spectra of representative samples are given in (Supplementary Fig. S1). The bands observed near 3400 cm^{-1} and 1630 cm^{-1} correspond to the O–H stretching and bending vibration of residual H_2O molecules absorbed from the environment [36]. The band in the wavenumber range of 400 to 600 cm^{-1} were assigned to the metal–oxygen–metal (Ce–O–Ni). A slight higher shift from 518 to 525 cm^{-1} is attributed to the nickel incorporation effect on ceria [37]. Textural properties of the catalysts are prescribed on Supplementary Table S2. After addition of Ni on ceria the pore diameter and surface area are increased.

TPD is an important tool to get an understanding of the surface nature/strength of acid-basic sites that act as active centers and their distribution that generally governs a catalytic reaction. Comparison of CO_2 TPD profile (CO_2-TPD) (Supplementary Fig. S2a) of ceria (0.010 mmol/g) and CN-10 (0.324 mmol/g) catalyst revealed the presence of larger number of moderate basic sites (250 to 350 °C) for the latter catalyst (with respect to ceria). Furthermore, NH_3-TPD [ceria (0.055 mmol/g) < CN-10 (0.482 mmol/g)] results have also suggested a significant increase in the number of weak (100–200 °C), moderate (230–400 °C) and strong (above 400 °C) acid sites upon introducing of Ni. Overall, the TPD results confirmed the presence of strong

acidic and moderate basic sites in CN-10 sample (Supplementary Fig. S2b) [12, 27, 38, 39]. Furthermore, to evaluate the distribution of Bronsted/Lewis acidic sites on ceria and CN-10 catalysts, these samples also analysed by pyridine-FTIR studies. From the B/L ratios presented in Supplementary Table S2 for CeO_2 and CN-10 samples. It is evident that introduction of NiO created additional strong Bronsted acid sites in agreement with the trends observed with NH_3 TPD (Supplementary Table S2) [40].

The Raman spectra of the synthesized pristine ceria showed a band at ~ 560 cm^{-1}, while CN-10 showed an intense band at ~ 40 cm^{-1} (Supplementary Fig. S3). The shift in the band towards lower wavenumber indicates an increase in the lattice distortion upon nickel incorporation and supports substitution and interstitial point defect [41]. Further, higher intensity of the band for CN-10 suggests the presence of more oxygen vacancy when compared to the bare CeO_2 [39]. In addition, weak and broad bands were observed at 215 cm^{-1} and 1100 cm^{-1} for CN-10 sample assigned to rhombohedra NiO. In general for NiO, rhombohedral vibrational bands occur at 1120 cm^{-1} [42]. This slight higher shift suggests that NiO is not present in free-state and interact with Ce in a plausible structural assembly as O–Ni–O–Ce [43]. FTIR also gave a strong support for metal–oxygen-metal arrangement by exhibiting bands in 400–600 cm^{-1} region (Supplementary Fig. S1). XPS of CN-10 samples were performed to understand the surface oxidation states of the elements present and their possible interactions. In both the cases, the deconvoluted (using AVANTAGE software with SMART background) 3d core level spectra of Ce was in the range of 878–925 eV with two sets of peaks confirm the presence of both Ce^{3+} and Ce^{4+} oxidation states (3d$_{5/2}$, 3d$_{3/2}$; Supplementary Figs. S4a, b and S5b). The peaks labelled as v′ and u′ correspond to Ce^{3+} and all other peaks labelled as v, v″, v‴, u, u″, and u‴ correspond to Ce^{4+} [44–47]. The relative weight percentage of [Ce^{3+}] and [Ce^{4+}] calculated by the Eq. 1 (SI) and observed the amount of [Ce^{3+}] as 17.6% and [Ce^{4+}] as 82.39%. Supplementary Fig. S4d is the Ni 2p high resolution scan which indicate the presence of nickel as NiO (854.9 eV) [48, 49]. The binding energies of oxygen on the surface were positioned at 528.7 eV, 531.5 eV, and 529.4 eV (Supplementary Fig. S4c). The peak centered at 528.7 eV corresponds to the oxygen bonded with cerium and 531.5 eV associated with oxygen bonded with nickel. Finally, 531.5 eV is usually attributed to the weakly absorbed oxygen species on the surface of CN-10 [44, 50]. HRTEM image of CN-10 sample confirm that material was high crystallinity and Ni in the + 2-oxidation state (Supplementary Fig. S7a–c).

Catalytic performance

Cerium oxide is a well-known heterogeneous oxidation catalyst due to the co-presence of stable Ce^{4+} and Ce^{3+} oxidation states [51, 52]. For the conversion of CO_2 to DMC as reported by many research groups [53], the ideal requirement for the reaction is the presence of dual active sites i.e. acidic sites to produce methyl cation from methanol and basic sites to produce methoxide anion (CH_3O^-) from methanol [54].

Considering previous literature reports, different mixed metal oxides were prepared and screened for the DMC formation. Pristine ceria catalyst (precipitation

Table 1 Catalyst screening for DMC synthesis

Entry	Catalyst[a]	DMC yield (mmol)	Selectivity (%)
1	CeO_2	0.6	100
2	$Ce_{0.9}Cu_{0.1}O_{2-\delta}$	0.2	98
3	$Ce_{0.9}Ni_{0.1}O_{2-\delta}$	3.6	100
4	$Ce_{0.9}Mg_{0.1}O_{2-\delta}$	0.4	94
5	$Ce_{0.9}Al_{0.1}O_{2-\delta}$	0.4	100
6	$Ce_{0.9}Zn_{0.1}O_{2-\delta}$	<0.1	100

[a]Catalysts are calcined at 600 °C at 4 h; Conditions: catalyst amount: 0.5 g, methanol: 20 g, CO_2-pressure: 40 bar, temperature: 150 °C, time: 4 h

method, SI) produced only 0.6 mmol of DMC under the studied conditions. Among the catalysts studied, nickel loaded cerium catalyst showed the highest yield of DMC (3.6 mmol) while all other dopants like copper, magnesium, aluminium and zinc showed lesser yield of DMC (Table 1). The higher yield obtained upon doping of nickel in the cerium oxide is possible to due to the generation of oxygen vacancies in the catalyst, which in turn enhance the CO_2 binding ability with the catalyst [55]. As Ni modified Ce catalyst gave the maximum yield, it was taken further for reaction parameters optimization.

The catalytic activities of different amounts of Ni-loaded ceria catalysts are given in Fig. 2a, which shows the Ce with 10% Ni loading (CN-10 catalyst) showed a maximum yield of DMC. While a further increase in nickel concentration decreased the yield of DMC. The observed decrease in DMC yield increased the curiosity to seek the role of Ni upon activity of ceria catalyst. It is a well-known fact that heterogeneous catalyst activity is generally influenced by the amount of desired active metal sites, surface oxygen and the type of defect induced by the foreign atom (doping). As shown in the Fig. 2a, beyond 10 % nickel loading on ceria resulted a decrease in the DMC yield. This may be due to the possibility of active site poison in the catalyst with higher amount of nickel (Fig S6). We believe, from the CO_2 and NH3-TPD analysis, the presence of large concentration of co-existing moderate basic and strong acidic sites in CN-10 is an important criterion for obtaining high yield of DMC. DFT studies makes solid evidence for the DMC yield improvement after addition of Ni (Supplementary Fig. S8). The adsorption energy of CO_2 and MeOH adsorbed on pristine ceria and Ni modified ceria are listed in Supplementary Table S3. The adsorption energy of CO_2 (-0.58 eV) and MeOH (-1.31 eV) on Ni modified ceria is less as compared to CO_2 (-0.37 eV) and MeOH (-1.24 eV) on pristine ceria. After adsorption, the bond length of the C–O and O–H are varying (Supplementary Table S3).

In order to improve the yield further, reaction parameters such as catalyst amount, temperature, time and CO_2 pressure were varied. To find out the optimum catalyst loading, different amounts of catalyst were used and the reaction was carried out (Fig. 2b). The results showed a maximum of 3.6 mmol DMC yield with 25 g/kg catalyst loading with respect to methanol. A further increase
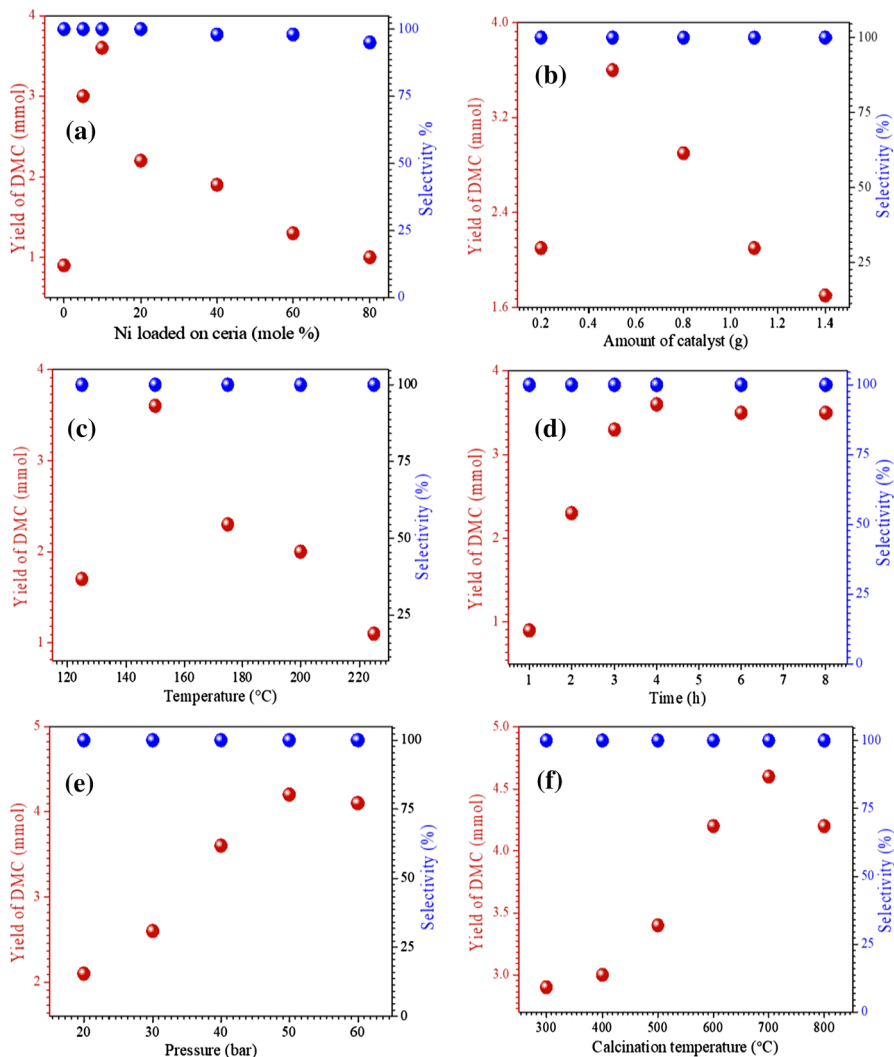
Fig. 2 Catalytic performance of **a** nickel loaded on ceria* (MeOH: 20 g, 40 (CO_2) bar, 150 °C, 4 h), **b** amount of catalyst* (MeOH: 20 g, 40 (CO_2) bar, 150 °C, 4 h), **c** temperature* (MeOH: 20 g, 40 (CO_2) bar, 4 h), **d** time* (MeOH: 20 g, 40 (CO_2) bar, 150 °C), **e** pressure (CO_2)* (MeOH: 20 g, 150 °C, 4 h), **f** calcination temperature (MeOH: 20 g, 50 (CO_2) bar, 150 °C, 4 h). *Catalyst was calcined at 600 °C at 4 h

in the catalyst loading results the drop in DMC yield. Catalyst amount plays a significant role in the catalytic activity by providing active sites for the reaction, however, the drop in yield may be attributed to the agglomeration, which is also observed in literature reports [56]. Thus, 25 g/kg catalyst loading was taken as optimum and the action was then carried out at different temperatures. Temperature variation studies (Fig. 2c) showed a maximum yield of 3.6 mmol

at 150 °C, and higher or lower than this temperature showed detrimental effect. Reaction time variation studies (Fig. 2d) revealed that 4 h is the optimum time to obtain maximum DMC yield. Further, extension of reaction time (8 h) has no effect. This indicates that DMC conversion in the equilibrium level [12, 13]. As reported earlier, the formation rate of DMC increased with increasing CO_2 pressure [57] therefore, a high CO_2 pressure is usually desirable for DMC synthesis. Further, increase in the pressure beyond 50 bar does not change the DMC formation (Fig. 2e). Thus, from the reaction parameter variation studies, 10% Ni amount, 25 g/kg catalyst loading, 150 °C, 4 h and 50 bar are found as the optimal reaction conditions to obtain the maximum yield of DMC. Further CN-10 catalyst was also taken and calcined at different temperatures and the reaction was conducted at optimized condition. The results revealed that, the catalyst calcined at lower temperature showed lesser DMC yield (~ 3 mmol) while increased with an increase in the calcination temperature (Fig. 2f). The yield enhancement is probably due to an increase in the crystalline nature of the catalyst. To validate, catalysts calcined at different temperatures were characterized by PXRD (Supplementary Fig. S9a). With increasing temperature, the crystallinity increased that correlated well with an increase in the DMC yield. Besides crystallinity, it is likely that the amount of surface oxygen species and defect formation propensity increase with an increase in calcination temperature [58]. However, with a further increase in calcination temperature (< 700 °C), a sharp decrease in the concentration of acidic sites occurs and thus in turn reduces the yield of DMC (Supplementary Fig. S9b). Furthermore, from the plots of DMC formation rate vs acidity/basicity (Supplementary Fig. S10), we observed clear co-relation between DMC formation rate and induced surface acidity/basicity in agreement with role of Ni upon creation additional defect sites. Furthermore, when CN-10 was calcined at elevated temperature (700 and 800 °C) it resulted in a decrease in basic site concentration. However, DMC formation rate for CN-10 (700 °C) and CN-10 (800 °C) samples remained almost unaffected. This observation indicated that DMC formation rate to be independent of basic site concentration, rather a synergistic combination of acidic/basic sites was essential for enhancing reaction rate.

Fig. 3 Recycling study of CN-10 catalyst calcined at 700 °C at 4 h; Conditions: methanol: 20 g, CO_2-pressure: 50 bar, temperature: 150 °C, time: 4 h
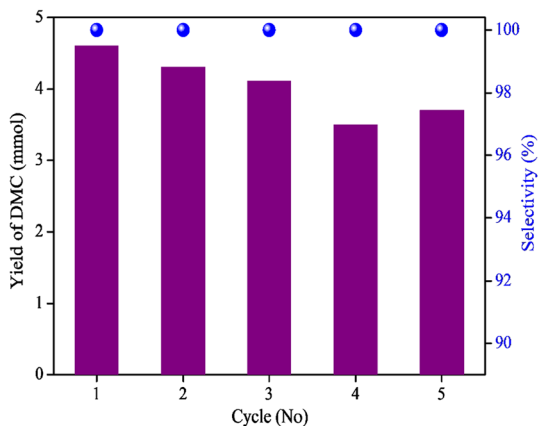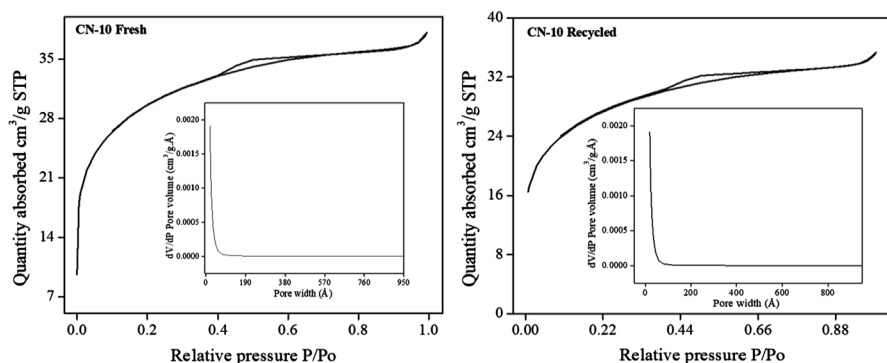
Fig. 4 BET surface area and pore volume of CN-10 fresh and 5th recycle catalyst of CN-10

Table 2 Effect of the synthetic method; 10 mol% nickel loaded ceria catalysts on activity

Entry	Synthesis method[a]	DMC yield (mmol)	Selectivity (%)
1	Precipitation	4.6	100
2	Impregnation	2.3	100
3	Hydrothermal	3.9	100
4	Ammonia evaporation + aging	3.8	100

[a]Catalyst are calcined at 700 °C at 4 h; Conditions: methanol: 20 g, CO_2-pressure: 50 bar, temperature: 150 °C, time: 4 h

The recyclability of the catalyst was assessed under optimized condition for up to five cycles. A slight decrease in the yield from 4.6 mmol in first use to 3.4 mmol in fifth use was observed (Fig. 3). To find out the plausible reason, PXRD, surface area and XPS was recorded for the recycled catalyst (Fig. 4 and Supplementary Figs. S11 and S5a). The PXRD of CN-10 catalyst turned amorphous upon recycling as evidenced by the decrease in the intensity of the characteristic reflections of ceria. As per XP spectra, no significant change in the nature of the peaks, clearly depicts similar surface distribution of elements after the catalytic cycle.

This result further corroborates the importance of the crystallinity of ceria catalyst on the activity. After the recycle the surface area slightly reduced from 101 to 91 m^2/g, because of the slight decrease the DMC yield also reduced (Fig. 4). 10 mol% Ni loaded on ceria catalyst was prepared by different synthesis protocol to understand the influence of synthesis methodology. Variation in the methodology influenced the DMC yield although all the methods rendered 100% selectivity wherein precipitation method showed the highest DMC yield (Table 2). Impregnation method showed low yield of DMC compared to other protocols augmented the necessity of moderate basic sites in enabling the catalytic activity for DMC synthesis (Supplementary Fig. S12).

Furthermore, the catalyst also be employed upon continuous vapour phase carboxylation of CO_2 with MeOH (Supplementary Fig. S13). Importantly the Ni

modified CeO_2 catalyst showed improved activity (DMC yield) and stability during 18 h TOS when compared to the pristine CeO_2 catalyst.

Conclusions

Ni-loaded cerium oxide catalysts with different concentration of Ni^{2+} were synthesized by simple co-precipitation and less time-consuming method followed by high-temperature calcination. A maximum yield of DMC in batch reactor (4.6 mmol) was observed for 10 mol% Ni loaded ceria catalyst at 150 °C using 50 bar CO_2 pressure in 4 h. The high activity of the catalyst (compared to pristine by six times) is due to the presence of high concentration of strong acid and moderate base sites as revealed from NH_3/CO_2-TPD measurements and Lewis/Bronsted sites as identified by pyridine adsorption measurements monitored using DRIFT FT-IR and Raman spectroscopy. The catalyst was recyclable for up to five cycles with a marginal drop in DMC yield owing to a decrease in the crystallinity. Among various preparation methods employed for Ni loaded ceria catalyst, precipitation synthetic protocol showed a maximum DMC yield. Reactions carried out under continuous flow showed superior activity of nickel loaded ceria (15 mmol) compared to the pristine ceria (5 mmol). DFT studies reveal that adsorption of CO_2 and methanol on Ni loaded ceria brings a considerable change in the geometrical parameters compared to pristine ceria thereby helps to improving the activity.

Declarations

Conflict of interest The authors declare that they have no conflict of interest.

References

1. Marjanović V, Milovančević M, Mladenović I (2016) Prediction of GDP growth rate based on carbon dioxide (CO_2) emissions. J. CO2 Util 16:212–217. https://doi.org/10.1016/j.jcou.2016.07.009
2. Zhou Y, Wang S, Xiao M, Han D, Lu Y, Meng Y (2015) Formation of dimethyl carbonate on nature clay supported bimetallic copper–-nickel catalysts. J Clean Prod 103:925–933. https://doi.org/10.1016/j.jclepro.2014.08.075
3. Zhang M, Xiao M, Wang S, Han D, Lu Y, Meng Y (2015) Cerium oxide-based catalysts made by template-precipitation for the dimethyl carbonate synthesis from carbon dioxide and methanol. J Clean Prod 103:847–853. https://doi.org/10.1016/j.jclepro.2014.09.024
4. Zhong CL, Guo XM, Mao DS, Wang S, Wu GS, Lu GZ (2015) Effects of alkaline-earth oxides on the performance of a CuO–ZrO$_2$ catalyst for methanol synthesis via CO_2 hydrogenation. RSC Adv 5:52958–52965. https://doi.org/10.1039/c5ra06508a

5. Bian J, Xiao M, Wang S-J, Lu Y-X, Meng Y-Z (2009) Carbon nanotubes supported Cu–Ni bimetallic catalysts and their properties for the direct synthesis of dimethyl carbonate from methanol and carbon dioxide. Appl Surf Sci 255:7188–7196. https://doi.org/10.1016/j.apsusc.2009.03.057

6. Subramanian S, Song Y, Kim D, Yavuz CT (2020) Redox and nonredox CO_2 utilization: dry reforming of methane and catalytic cyclic carbonate formation. ACS Energy Lett 5:1689–1700. https://doi.org/10.1021/acsenergylett.0c00406

7. Cao YX, Cheng HX, Ma LL, Liu F, Liu ZM (2012) Research progress in the direct synthesis of dimethyl carbonate from CO_2 and methanol. Catal Surv Asia 16:138–147. https://doi.org/10.1007/s10563-012-9140-5

8. Zhu SH, Gao XQ, Zhu YL, Fan WB, Wang JG, Li YW (2015) A highly efficient and robust Cu/SiO_2 catalyst prepared by the ammonia evaporation hydrothermal method for glycerol hydrogenolysis to 1,2-propanediol. Catal Sci Technol 5:1169–1180. https://doi.org/10.1039/c4cy01148a

9. Sankaranarayanan S, Srinivasan K (2012) Carbon dioxide—a potential raw material for the production of fuel, fuel additives and bio-derived chemicals. Indian J. Chem. Sect. A Inorg Phys Theor Anal Chem 51:1252–1262

10. Fang SN, Fujimoto K (1996) Direct synthesis of dimethyl carbonate from carbon dioxide and methanol catalyzed by base. Appl Catal A Gen 142:L1–L3. https://doi.org/10.1016/0926-860x(96)00081-6

11. Huang CH, Tan CS (2014) A review: CO_2 utilization. Aerosol Air Qual Res 14:480–499. https://doi.org/10.4209/aaqr.2013.10.0326

12. Yoshida Y, Arai Y, Kado S, Kunimori K, Tomishige K (2006) Direct synthesis of organic carbonates from the reaction of CO_2 with methanol and ethanol over CeO_2 catalysts. Catal Today 115:95–101. https://doi.org/10.1016/j.cattod.2006.02.027

13. Tomishige K, Furusawa Y, Ikeda Y, Asadullah M, Fujimoto K (2001) CeO_2–ZrO_2 solid solution catalyst for selective synthesis of dimethyl carbonate from methanol and carbon dioxide. Catal Lett 76:71–74. https://doi.org/10.1023/A:1016711722721

14. Tomishige K, Kunimori K (2002) Catalytic and direct synthesis of dimethyl carbonate starting from carbon dioxide using CeO_2–ZrO_2 solid solution heterogeneous catalyst: effect of H_2O removal from the reaction system. Appl Catal A Gen 237:103–109. https://doi.org/10.1016/S0926-860x(02)00322-8

15. Santos BAV, Silva VMTM, Loureiro JM, Rodrigues AE (2014) Review for the direct synthesis of dimethyl carbonate. ChemBioEng Rev 1:214–229. https://doi.org/10.1002/cben.201400020

16. Dibenedetto A, Angelini A, Stufano P (2014) Use of carbon dioxide as feedstock for chemicals and fuels: homogeneous and heterogeneous catalysis. J Chem Technol Biotechnol 89:334–353. https://doi.org/10.1002/jctb.4229

17. Honda M, Sonehara S, Yasuda H, Nakagawa Y, Tomishige K (2011) Heterogeneous CeO_2 catalyst for the one-pot synthesis of organic carbamates from amines, CO_2 and alcohols. Green Chem 13:3406–3413. https://doi.org/10.1039/c1gc15646b

18. Honda M, Kuno S, Begum N, Fujimoto K, Suzuki K, Nakagawa Y, Tomishige K (2010) Catalytic synthesis of dialkyl carbonate from low pressure CO_2 and alcohols combined with acetonitrile hydration catalyzed by CeO_2. Appl Catal A Gen 384:165–170. https://doi.org/10.1016/j.apcata.2010.06.033

19. Akune T, Morita Y, Shirakawa S, Katagiri K, Inumaru K (2018) ZrO_2 nanocrystals as catalyst for synthesis of dimethylcarbonate from methanol and carbon dioxide: catalytic activity and elucidation of active sites. Langmuir 34:23–29. https://doi.org/10.1021/acs.langmuir.7b01294

20. Fu Z, Zhong Y, Yu Y, Long L, Xiao M, Han D, Wang S, Meng Y (2018) TiO_2-doped CeO_2 nanorod catalyst for direct conversion of CO_2 and CH_3OH to dimethyl carbonate: catalytic performance and kinetic study. ACS Omega 3:198–207. https://doi.org/10.1021/acsomega.7b01475

21. Prymak I, Prymak O, Wang J, Kalevaru VN, Martin A, Bentrup U, Wohlrab S (2018) Phosphate functionalization of CeO_2–ZrO_2 solid solutions for the catalytic formation of dimethyl carbonate from methanol and carbon dioxide. ChemCatChem 10:391–394. https://doi.org/10.1002/cctc.201701105

22. Han D, Chen Y, Wang S, Xiao M, Lu Y, Meng Y (2018) Effect of alkali-doping on the performance of diatomite supported Cu–Ni bimetal catalysts for direct synthesis of dimethyl carbonate. Catalysts. https://doi.org/10.3390/catal8080302

23. Kumar P, With P, Srivastava VC, Shukla K, Gläser R, Mishra IM (2016) Dimethyl carbonate synthesis from carbon dioxide using ceria–zirconia catalysts prepared using a templating method:

characterization, parametric optimization and chemical equilibrium modeling. RSC Adv 6:110235–110246. https://doi.org/10.1039/c6ra22643d

24. Hang GQ, Sun YC, Shi YB, Zheng HY, Li Z, Ju SG, Liu SJ, Shi PZ (2020) Surface properties of $Ce_{1-x}Mn_xO_2$ catalyst on the catalytic activities for direct synthesis of DMC from CO_2 and methanol. Chem Res Chin Univ 41:2061–2069. https://doi.org/10.7503/cjcu20200250

25. Deerattrakul V, Panitprasert A, Puengampholsrisook P, Kongkachuichay P (2020) Enhancing the dispersion of Cu–Ni metals on the graphene aerogel support for use as a catalyst in the direct synthesis of dimethyl carbonate from carbon dioxide and methanol. ACS Omega 5:12391–12397. https://doi.org/10.1021/acsomega.0c0114

26. Lee HJ, Joe W, Jung JC, Song IK (2012) Direct synthesis of dimethyl carbonate from methanol and carbon dioxide over Ga_2O_3–CeO_2–ZrO_2 catalysts prepared by a single-step sol–gel method: Effect of acidity and basicity of the catalysts. Korean J Chem Eng 29:1019–1024. https://doi.org/10.1007/s11814-012-0017-0

27. Tomishige K, Yasuda H, Yoshida Y, Nurunnabi M, Li B, Kunimori K (2004) Catalytic performance and properties of ceria based catalysts for cyclic carbonate synthesis from glycol and carbon dioxide. Green Chem. https://doi.org/10.1039/b401215a

28. Fu ZW, Yu YH, Li Z, Han DM, Wang SJ, Xiao M, Meng YZ (2018) Surface reduced CeO_2 nanowires for direct conversion of CO_2 and methanol to dimethyl carbonate: catalytic performance and role of oxygen vacancy. Catalysts. https://doi.org/10.3390/catal8040164

29. Tamboli AH, Chaugule AA, Gosavi SW, Kim H (2018) Ce $Zr_{1-x}O_2$ solid solutions for catalytic synthesis of dimethyl carbonate from CO_2: reaction mechanism and the effect of catalyst morphology on catalytic activity. Fuel 216:245–254. https://doi.org/10.1016/j.fuel.2017.12.008

30. Becke AD (1993) Density-functional thermochemistry. III. The role of exact exchange. J Chem Phys 98:5648–5652. https://doi.org/10.1063/1.464913

31. Stephens PJ, Devlin FJ, Chabalowski CF, Frisch MJ (1994) Ab initio calculation of vibrational absorption and circular dichroism spectra using density functional force fields. J Chem Phys 98:11623–11627. https://doi.org/10.1021/j100096a001

32. Lee C, Yang W, Parr RG (1988) Development of the colle-salvetti correlation-energy formula into a functional of the electron density. Phys Rev B 37:785–789. https://doi.org/10.1103/physrevb.37.785

33. Frisch MJ, Trucks GW, Schlegel HB, Scuseria GE, Robb MA, Cheeseman JR, Scalmani G, Barone V, Petersson GA, Nakatsuji H, Li X, Caricato M, Marenich AV, Bloino J, Janesko BG, Gomperts R, Mennucci B, Hratchian HP, Ortiz JV, Izmaylov AF, Sonnenberg JL, Williams, Ding F, Lipparini F, Egidi F, Goings J, Peng B, Petrone A, Henderson T, Ranasinghe D, Zakrzewski VG, Gao J, Rega N, Zheng G, Liang W, Hada M, Ehara M, Toyota K, Fukuda R, Hasegawa J, Ishida M, Nakajima T, Honda Y, Kitao O, Nakai H, Vreven T, Throssell K, Montgomery Jr. JA, Peralta JE, Ogliaro F, Bearpark MJ, Heyd JJ, Brothers EN, Kudin KN, Staroverov VN, Keith TA, Kobayashi R, Normand J, Raghavachari K, Rendell AP, Burant JC, Iyengar SS, Tomasi J, Cossi M, Millam JM, Klene M, Adamo C, Cammi R, Ochterski JW, Martin RL, Morokuma K, Farkas O, Foresman JB, Fox DJ (2016) Gaussian 16 Rev. C.01. Wallingford

34. Phokha S, Pinitsoontorn S, Chirawatkul P, Poo-Arporn Y, Maensiri S (2012) Synthesis, characterization, and magnetic properties of monodisperse CeO_2 nanospheres prepared by PVP-assisted hydrothermal method. Nanoscale Res Lett 7:425. https://doi.org/10.1186/1556-276X-7-425

35. Ginting M, Taslima S, Sebayang K, Aryanto D, Sudiro T, Sebayang P (2017) Preparation and characterization of zinc oxide doped with ferrite and chromium. AIP Conf Proc 1862:030062. https://doi.org/10.1063/1.4991166

36. Ansari A, Ali A, Asif M, Shamsuzzaman S (2018) Microwave-assisted MgO NP catalyzed one-pot multicomponent synthesis of polysubstituted steroidal pyridines. New J Chem 42:184–197. https://doi.org/10.1039/c7nj03742b

37. Ansari ZA, Athar T, Fouad H, Ansari SG (2017) Sol-Gel synthesis of manganese doped titanium oxide nanoparticles for electrochemical sensing of hydroquinone. J Nanosci Nanotechnol 17:2296–2301. https://doi.org/10.1166/jnn.2017.13855

38. Azzouz A, Nistor D, Miron D, Ursu AV, Sajin T, Monette F, Niquette P, Hausler R (2006) Assessment of acid-base strength distribution of ion-exchanged montmorillonites through NH3 and CO_2-TPD measurements. Thermochim Acta 449:27–34. https://doi.org/10.1016/j.tca.2006.07.019

39. Taniguchi T, Watanabe T, Sugiyama N, Subramani AK, Wagata H, Matsushita N, Yoshimura M (2009) Identifying defects in ceria-based nanocrystals by UV resonance raman spectroscopy. J Phys Chem C 113:19789–19793. https://doi.org/10.1021/jp9049457

40. Nakajima K, Noma R, Kitano M, Hara M (2013) Titania as an early transition metal oxide with a high density of lewis acid sites workable in water. J Phys Chem C 117:16028–16033. https://doi.org/10.1021/jp404523r
41. Yisup N, Cao Y, Feng W-L, Dai W-L, Fan K-N (2005) Catalytic oxidation of methane over novel Ce–Ni–O mixed oxide catalysts prepared by oxalate gel-coprecipitation. Catal Lett 99:207–213. https://doi.org/10.1007/s10562-005-2121-9
42. Mironova-Ulmane N, Kuzmin A, Steins I, Grabis J, Sildos I, Pärs M (2007) Raman scattering in nanosized nickel oxide NiO. J Phys Conf Ser. https://doi.org/10.1088/1742-6596/93/1/012039
43. Pal P, Singha RK, Saha A, Bal R, Panda AB (2015) Defect-induced efficient partial oxidation of methane over nonstoichiometric Ni/CeO$_2$ nanocrystals. J Phys Chem C 119:13610–13618. https://doi.org/10.1021/acs.jpcc.5b01724
44. Li P, Zhang M, Li X, Wang C, Wang R, Wang B, Yan H (2020) MOF-derived NiO/CeO$_2$ heterojunction: a photocatalyst for degrading pollutants and hydrogen evolution. J Mater Sci 55:15930–15944. https://doi.org/10.1007/s10853-020-05123-2
45. Zou W, Ge C, Lu M, Wu S, Wang Y, Sun J, Pu Y, Tang C, Gao F, Dong L (2015) Engineering the NiO/CeO$_2$ interface to enhance the catalytic performance for CO oxidation. RSC Adv 5:98335–98343. https://doi.org/10.1039/c5ra20466f
46. Xue S-F, Wu W-Y, Bian X, Wang Z-F, Wu Y-F (2018) Facile preparation of CeO$_2$ microspheres with high surface area by ultrasonic spray pyrolysis. Green Process Synth 7:241–247. https://doi.org/10.1515/gps-2017-0041
47. Lian J, Liu P, Jin C, Shi Z, Luo X, Liu Q (2019) Perylene diimide-functionalized CeO$_2$ nanocomposite as a peroxidase mimic for colorimetric determination of hydrogen peroxide and glutathione. Mikrochim Acta 186:332. https://doi.org/10.1007/s00604-019-3439-0
48. Bear J, McNaughter P, Southern P, O'Brien P, Dunnill C (2015) Nickel-doped ceria nanoparticles: the effect of annealing on room temperature ferromagnetism. Curr Comput-Aided Drug Des 5:312–326. https://doi.org/10.3390/cryst5030312
49. Cui J, Luo J, Peng B, Zhang X, Zhang Y, Wang Y, Qin Y, Zheng H, Shu X, Wu Y (2016) Synthesis of porous NiO/CeO$_2$ hybrid nanoflake arrays as a platform for electrochemical biosensing. Nanoscale 8:770–774. https://doi.org/10.1039/c5nr05924k
50. Fifere N, Airinei A, Dobromir M, Sacarescu L, Dunca SI (2021) Revealing the effect of synthesis conditions on the structural, optical, and antibacterial properties of cerium oxide nanoparticles. Nanomaterials. https://doi.org/10.3390/nano11102596
51. Zhang F, Wang P, Koberstein J, Khalid S, Chan S-W (2004) Cerium oxidation state in ceria nanoparticles studied with X-ray photoelectron spectroscopy and absorption near edge spectroscopy. Surf Sci 563:74–82. https://doi.org/10.1016/j.susc.2004.05.138
52. Reddy BM, Kumar TV, Durgasri N (2013) New developments in ceria-based mixed oxide synthesis and reactivity in combustion and oxidation reactions. In: Trovarelli A, Fornasiero P (eds) Catalysis by ceria and related materials. Imperial College Press, London, pp 397–464
53. Tamura M, Honda M, Nakagawa Y, Tomishige K (2014) Direct conversion of CO$_2$ with diols, aminoalcohols and diamines to cyclic carbonates, cyclic carbamates and cyclic ureas using heterogeneous catalysts. Catal Commun 89:19–33. https://doi.org/10.1002/jctb.4209
54. Almusaiteer K (2009) Synthesis of dimethyl carbonate (DMC) from methanol and CO$_2$ over Rh-supported catalysts. Catal Commun 10:1127–1131. https://doi.org/10.1016/j.catcom.2009.01.012
55. Razzaq R, Zhu HW, Jiang L, Muhammad U, Li CS, Zhang SJ (2013) Catalytic methanation of CO and CO$_2$ in coke oven gas over Ni–Co/ZrO$_2$–CeO$_2$. Ind Eng Chem Res 52:2247–2256. https://doi.org/10.1021/ie301399z
56. Albers P, Pietsch J, Parker SF (2001) Poisoning and deactivation of palladium catalysts. J Mol Catal A Chem 173:275–286. https://doi.org/10.1016/s1381-1169(01)00154-6
57. Honda M, Suzuki A, Noorjahan B, Fujimoto K, Suzuki K, Tomishige K (2009) Low pressure CO$_2$ to dimethyl carbonate by the reaction with methanol promoted by acetonitrile hydration. Chem Commun 30:4596–4598. https://doi.org/10.1039/b909610h
58. Harrison PG, Ball IK, Azelee W, Daniell W, Goldfarb D (2000) Nature and surface redox properties of copper(II)-promoted cerium(IV) oxide CO-oxidation catalysts. Chem Mater 12:3715–3725. https://doi.org/10.1021/cm001113k